International Journal of Mechanical, Industrial and Aerospace Sciences
ISSN: 2517-9950
Vol:1, No:8, 2007

CQAR: Closed Quarter Aerial Robot Design for Reconnaissance, Surveillance and Target Acquisition Tasks in Urban Areas

Paul Y. Oh and William E. Green

Abstract — This paper describes a prototype aircraft that can fly slowly, safely and transmit wireless video for tasks like reconnaissance, surveillance and target acquisition. The aircraft is designed to fly in closed quarters like forests, buildings, caves and tunnels which are often spacious but GPS reception is poor. Envisioned is that a small, safe and slow flying vehicle can assist in performing dull, dangerous and dirty tasks like disaster mitigation, search-and-rescue and structural damage assessment.

Keywords — Unmanned aerial vehicles, autonomous collision avoidance, optic flow, near-Earth environments

I. Introduction

Unmanned aerial vehicles like General Atomics' Predator is an airborne surveillance system equipped with a full suite of sensors like GPS, inertial measurement units, laser range finders and computer vision to perform tasks like reconnaissance and target acquisition. Called UAVs, such teleoperated aircraft fly in open skies. In contrast, our particular interests are designing aerial robots that fly in *closed quarters* – near-Earth environments like forests, buildings, train stations, caves and tunnels, which are spacious but cluttered. The challenges in flying in such environments are compounded by the fact that GPS is poor, communications are degraded and lighting is unpredictable. A robotic aircraft that can overcome such challenges and fly autonomously in closed quarters would be a useful surveillance tool for dismounted soldiers, search-and-rescue workers and first responders. As such, our design goal is a flying robot we call CQAR: *Closed Quarter Aerial Robot* (pronounced "seeker") that can patrol near-Earth environments. A 30-gram fixed-wing prototype (see Figure 1) that flies 2 m/s with a 30-inch wing span is featured.

This paper's objective is to formulate and provide a set of guidelines in designing an aerial robot to fly in closed quarters, in and around buildings and possibly tunnels and caves. Section II features the pros, cons and underlying dynamics contrasting lighter-than-air, rotary and fixed wing vehicles. Sections III and IV respectively present design optimization and the current prototype. Section V presents a 14-gram avionics package consisting of an optic flow sensor and motor controller. Autonomous flight behaviors like collision avoidance [14] and landing [9] are featured. Section VI concludes and outlines near-future goals.

Manuscript received March 25, 2004. This material is based upon work supported by the National Science Foundation under CAREER Grant No. 0347430. Any opinions, findings, and conclusions or recommendations expressed in this material are those of the author(s) and do not necessarily reflect the views of the National Science Foundation.

Paul Y. Oh (corresponding author) is the Director of the Autonomous Systems Lab at Drexel University, Mechanical Engineering & Mechanics, 3141 Chestnut Street, Philadelphia PA USA, 19038 Tel: 215-895-6396, Fax: 215-895-1478, Email: paulcoe.drexel.edu

William E. Green is with Drexel University Mechanical Engineering, 3141 Chestnut Street, Philadelphia PA USA, 19038 Email: weg22drexel.edu

II. Flight Modes

Lighter-than-air vehicles like blimps, rotorcraft like helicopters, fixed and flapping wing aircraft and tethered devices like kites [15] retrofitted with sensor suites are detailed in the aerial robotics literature. This section highlights and summarizes the underlying pros, cons and dynamics for various flight modes. Kites are not suited for closed quarters and are not discussed in this paper. Ornithopters [6], which show some promise, are currently being assessed and will be the subject of a future paper.

A. Lighter-than-air Vehicles

The most common gas used today in blimps is Helium, which has a lifting capacity of 0.064 lbs/ft3 (1.02 kg/m3). The helium makes the blimp positively buoyant in the surrounding air so that the blimp rises. Because gas provides the sufficient lifting force in blimps rather than wings and electric motors, blimps can remain airborne without expending fuel. This allows them to hover in the air for hours and days at a time, which is significantly longer than rotary and fixed wing aircraft. The disadvantage for using blimps in closed quarters, however, is that a blimp's buoyancy and inertial forces are proportional to its size. When flying in closed quarters for surveillance or search and rescue applications, it is essential to have a vehicle that can easily fit through a standard 3 foot doorway or maneuver easily around pillars and hanging lights. Furthermore, because of its large inertial force, it is not able to quickly reverse directions.

Figure 2 depicts a free body diagram of a gondola attached to a Helium-filled blimp. The gondola sits below the center of gravity and hence most of the pitch and roll motion will be negligible (Zhang and Ostrowski [21]). The four forces acting on the blimp during flight are buoyancy B, drag D, thrust T and weight W. The blimp is assumed to be in mid-flight and the z-axis (in the direction opposite of gravity), x-axis (parallel to the ground) and forces of buoyancy, drag and weight intersect at the center of buoyancy. The thrust forces act at the locations of the propellers and α is the angle the propeller shafts make with the x-axis. The drag force is in

Fig. 1. Closed quarters like this train station are enclosed but spacious for aerial robots. An aircraft that is small, safe and flies slowly can navigate down halls and around obstacles

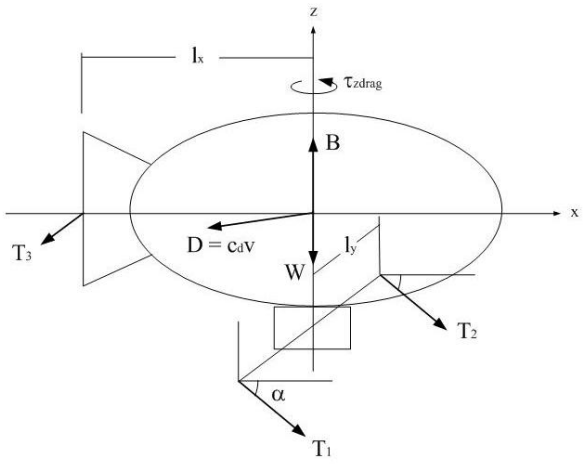

Fig. 2. Blimp force diagram

the direction opposite of motion. The equations of motion for a blimp are statements of Newton's second law, F=ma. The blimp's equations of motion are:

$$\begin{aligned} m_x a_x &= (T_1 + T_2)\cos\alpha - D_x \\ m_z a_z &= D_z + (T_1 + T_2)\sin\alpha \\ J_z \dot{\omega}_z &= (T_1 - T_2) l_y \cos\alpha + T_3 l_x + \tau_{z\text{drag}} \end{aligned}$$

B. Rotary Wing Aircraft

Rotary wing aircraft, like helicopters, are versatile, possessing the capability to hover and fly laterally and backwards. Such aircraft are much more complicated to fly than airplanes or blimps. Another downfall to the rotary wing machine is cost. The cost of materials to construct an airworthy model is substantially more expensive than conventional fixed wing aircraft materials. This is partly due to helicopters being much less stable in the air than airplanes and therefore more sophisticated mechanisms are required to increase stability, like tilt-rotor systems

Ducted fan units [4] like the organic air vehicle constructed for DARPA (Defense Advanced Research Projects Agency) in the United States both hover and translate. Its capabilities are very similar to a conventional helicopter. Several challenges include reducing fan noise, increasing flight duration and maintaining stability especially in the presence of ground-effect.

The dynamics of rotary wing aircraft are slightly more complex than lighter than air vehicles because of the tilt-rotor mechanisms they possess. Unlike lighter-than-air vehicles, which use helium, and fixed wing aircraft, which rely on wings to generate lift, a helicopter's main rotor supplies both the lift and thrust for the vehicle. This is achieved by tilting the rotor forward and the resolved forces move the aircraft horizontally while sustaining the required lift. The helicopter is assumed to be a rigid body in 3D space in order to streamline the dynamics. That is, when the rotor tilts, so does the fuselage. This is not unrealistic because in normal operations, the tail rotor is used to align the body with the flight direction to save fuselage drag. The free-body diagram of a helicopter in flight is shown in Figure 3. θ, Ψ and ϕ are the rigid body rotations about the x-axis, y-axis and z-axis respectively. The thrust T, drag D and weight W forces are assumed to be acting about the center of gravity. τ_1 and τ_2 are the rotor reaction forces and ε is the angle between the free-stream velocity and the horizontal thrust vector. J is the moment of inertia about the helicopter's center-of-gravity. Thus the equations of motion are

$$\begin{aligned} m_x a_x &= T\cos\theta\sin\Psi\cos\phi - D\cos\varepsilon\cos\theta\cos\Psi\cos\phi \\ &\quad + F_{3_x} \\ m_y a_y &= -T\sin\theta\cos\Psi\cos\phi + D\cos\varepsilon\cos\theta\cos\Psi\sin\phi \\ &\quad + F_{3_y} \\ m_z a_z &= T\cos\theta\cos\Psi\cos\phi + D\cos\varepsilon\cos\theta\sin\Psi\cos\phi \\ &\quad + F_{3_z} - W \end{aligned}$$

$$\begin{aligned} J_x\dot{\omega}_x &= \tau_{1_x} + \tau_{2_x} + F_{3_z} l_y + F_{3_y} l_z \\ J_y\dot{\omega}_y &= \tau_{1_y} + \tau_{2_y} + F_{3_z} l_x + F_{3_x} l_z \\ J_z\dot{\omega}_z &= \tau_{1_z} + \tau_{2_y} + F_{3_x} l_y + F_{3_y} l_x \end{aligned}$$

C. Fixed-wing Aircraft

Literature describing the design of fixed wing aircraft is vast with a long history. Such aircraft are also both more cost efficient and stable than their rotary wing counterparts. The governing design principle is that an aircraft's weight is proportional to its cruise velocity

$$W = \frac{1}{2}\rho V^2 S C_L \tag{1}$$

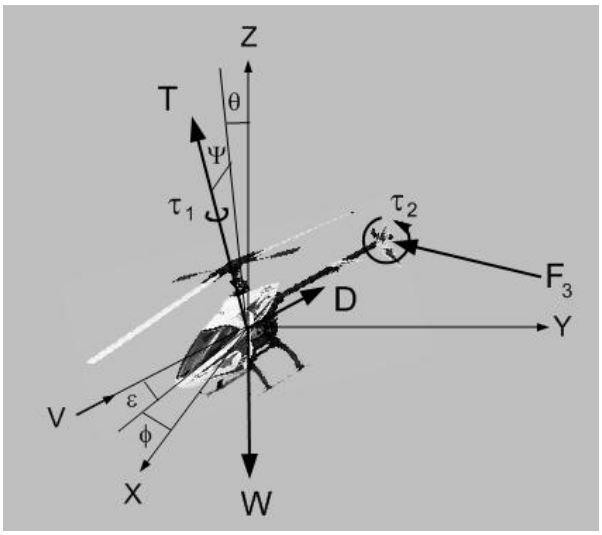

Fig. 3. Free-body diagram of helicopter

Fig. 4. Fixed-wing prototype prop hanging with a large angle-of-attack

Therefore, the lighter the aircraft, the lower the velocity requirements to maintain steady and level flight. Lower velocity requirements also correspond to higher maneuverability, which is crucial for closed quarters. Until recently, the largest restriction for fixed wing aircraft has been their inability to hover. However, slow speed aerodynamics permits large angles-of-attack without stall. For example, small light aircraft can perform an aerobatic maneuver called prop hanging which mimics hovering partially. Here, aircraft pitch and thrust are simultaneously increased. This results in the aircraft translating while having a near vertical pose (see Figure 4).

Micro air vehicles (MAV) are often defined having a size less than 6 inches in length, width and height, weighing less than 50 grams, having an endurance of 20 to 60 minutes for 6 miles and flying speeds ranging from 20 to 40 mph [8]. Military reconnaissance, such as gathering enemy information just over a hill or battlefield assessment in urban environments, is the primary application of a MAV. Although the size of a MAV is well suited for closed quarters, flying speed is too fast.

The vehicle dynamics for fixed wing aircraft are very similar

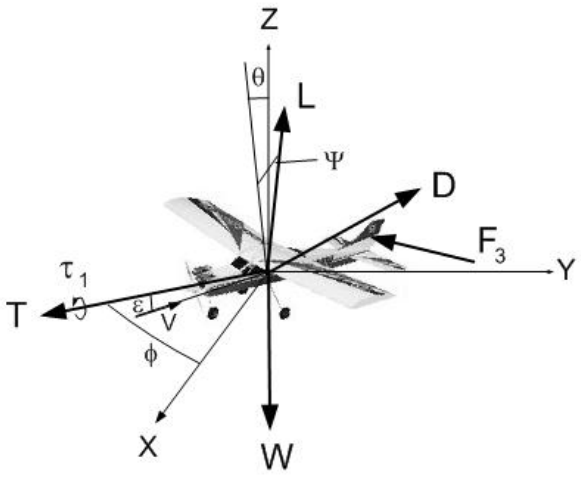

Fig. 5. Free-body diagram of fixed-wing vehicle

to their rotary wing counterparts when assumed to be rigid bodies [1]. The only differences are the propeller location and the absence of the tail rotor. However, the airplane's rudder and elevator compensate for this. The four forces of flight on a fixed wing aircraft are lift L, drag D, thrust T and weight W and are sketched in Figure 5. θ, Ψ and ϕ are the rigid body rotations about the x, y and z axes respectively. τ_1 is the propeller's reaction force and the angle between the free-stream velocity and the thrust vector is ε. The four forces of flight and the moment of inertia J are about the airplane's center of gravity. Thus, the Newtonian equations of motion for a fixed wing aircraft in three-dimensional space are:

$$\begin{aligned} m_x a_x &= T\cos\theta\cos\Psi\cos\phi - D\cos\varepsilon\cos\theta\cos\Psi\cos\phi \\ &\quad -L\cos\theta\sin\Psi\cos\phi + F_{3_x} \\ m_y a_y &= -T\cos\theta\cos\Psi\sin\phi + D\cos\varepsilon\cos\theta\cos\Psi\sin\phi \\ &\quad -L\sin\theta\cos\Psi\cos\phi + F_{3_y} \\ m_z a_z &= T\cos\theta\sin\Psi\cos\phi - D\cos\varepsilon\cos\theta\sin\Psi\cos\phi \\ &\quad -W + L\cos\theta\cos\Psi\cos\phi + F_{3_z} \end{aligned}$$

$$\begin{aligned} J_x\dot{\omega}_x &= \tau_{1_x} + F_{3_z}l_y + F_{3_y}l_z \\ J_y\dot{\omega}_y &= \tau_{1_y} + F_{3_z}l_x + F_{3_x}l_z \\ J_z\dot{\omega}_z &= \tau_{1_z} + F_{3_x}l_y + F_{3_y}l_x \end{aligned}$$

It can be seen from the equations above that $L = W$ and $T = D$ during cruise flight ($a_x = a_y = a_z = \theta = \Psi = \phi = 0$). Now that the pros, cons and dynamics of each model are accounted for, metrics for a design matrix can be formulated.

III. Optimal Design Matrix

A closed quarter aerial robot demands understanding how aerodynamics, sensor suite integration and task influence design. The pros, cons and underlying dynamics presented in the previous section can be parameterized into design variables. Towards this a multi-disciplinary design optimization (MDO) matrix (Grasmeyer, Keennon [8]) is very helpful. The MDO method originated in the automobile industry [11] and has evolved into an invaluable discipline that supplies engineers with techniques to move engineering system design closer

to optimal. Inputting some initial components into a design matrix will yield the most applicable platform and its corresponding equations of motion.

Each design variable used has a large impact on platform selection (see Figure 6). The parameters that make up the design matrix include initial variables X_I, velocity variables X_V, size variables X_S, payload variables X_P, and hover variables X_H. The initial variables determine the mission type and include parameters such as environment (closed quarter, outdoors or both), desired tasks (search and rescue or reconnaissance), expendability, vertical takeoff and landing requirements, and stealthy operation. The velocity parameters are used to establish speed range capabilities. The size variables represent the platforms maximum characteristic length as well as propeller diameter. This will conclude whether or not the vehicle can fit through small openings like doorways. Payload variables determine the weight and dimensions of the designed sensor suite. The hover parameters assess whether or not there is a requirement and also the endurance of the hover. Common input parameters such as flight endurance, range or propeller geometry were not selected in this design matrix because such parameters can be manipulated once the optimal platform is selected.

Based on the input parameters specified above, the program executes a series of commands to generate the most suitable aerial platform and its corresponding equations of motion. A graphical representation for the command sequence is shown in a flow chart (see Figure 7). The shaded boxes represent the input parameters of the user. Initially, a closed quarter environment and a search and rescue mission were specified which did not rule out any of the platforms. Next, the user wanted something that was expendable (roughly less than 300 USD) which eliminated more expensive rotorcraft as a possible solution for this mission. VTOL and stealthy operations were not required and consequently, lighter than air vehicles and fixed wing aircraft still remain. A velocity range (min to max) of 5 to 10 MPH was specified and likewise did not eradicate any of the remaining. However, because the maximum characteristic length was selected as less than 18-inches, lighter than air vehicles were eliminated (size is proportional to lift force) and fixed wing aircraft was outputted as the optimal platform. All MAVs and most small fixed wing vehicles can fly with a wing span less than 18-inches. Furthermore, the design matrix also yielded the platform dynamics which will allow the user to get an estimate of the aircraft's weight based on the inputs to the velocity matrix from (1). By selecting the most suitable aircraft and outputting its aerodynamic data, the MDO matrix will allow a more theoretical approach to the design and development of small autonomous aircraft prototypes.

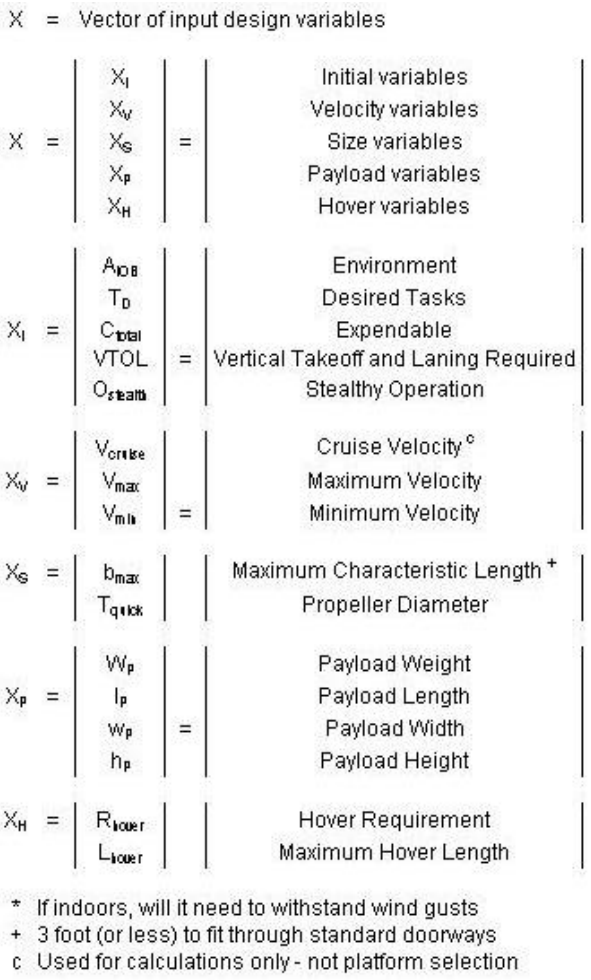

Fig. 6. Design matrix input parameters

IV. CQAR Prototype

A prototype based on the output from the design optimization matrix was constructed. The design demanded a fixed-wing flight mode with a maximum wing span of 46 cm and 26 g mass (about 3 U.S. quarter coins). The resulting vehicle would be able to carry a 14 g sensor payload and navigate in a 10×10 m^2 area (about $1/3$ the size of a basketball court) when flying at a maximum speed of 2 m/s (about the speed of a slow jogging person).

The equations of motion ($L = W$ during cruise) generated by the design matrix allowed us to calculate the wing loading (W/S) for our aircraft (with a lift coefficient $C_L = 1$) using (1). A graph was then created for several wing loading scenarios (see Figure 8). From the graph, it can be seen that a weight of less than 30 g was required to fly in a room that is 10 m long. This gives the sensors and control system 5 s of time to react and accomplish a turn when flying at the 2 m/s maximum speed.

The fuselage and airfoil frame were constructed out of carbon fiber rods with a 3 μm mylar covering, while the tail is made from mylar covered balsa wood. With a payload capacity of 14 g, the aircraft can carry a light-weight mini wireless camera and power supply as shown in Figure 9 (left). The middle photo is a frame captured by the on-board camera while flying in the atrium. A table can be identified, but the image is noisy. For comparison, the actual table is depicted in the right photo. The noise is due to both interference from the university's 802.11b wireless network and the wireless

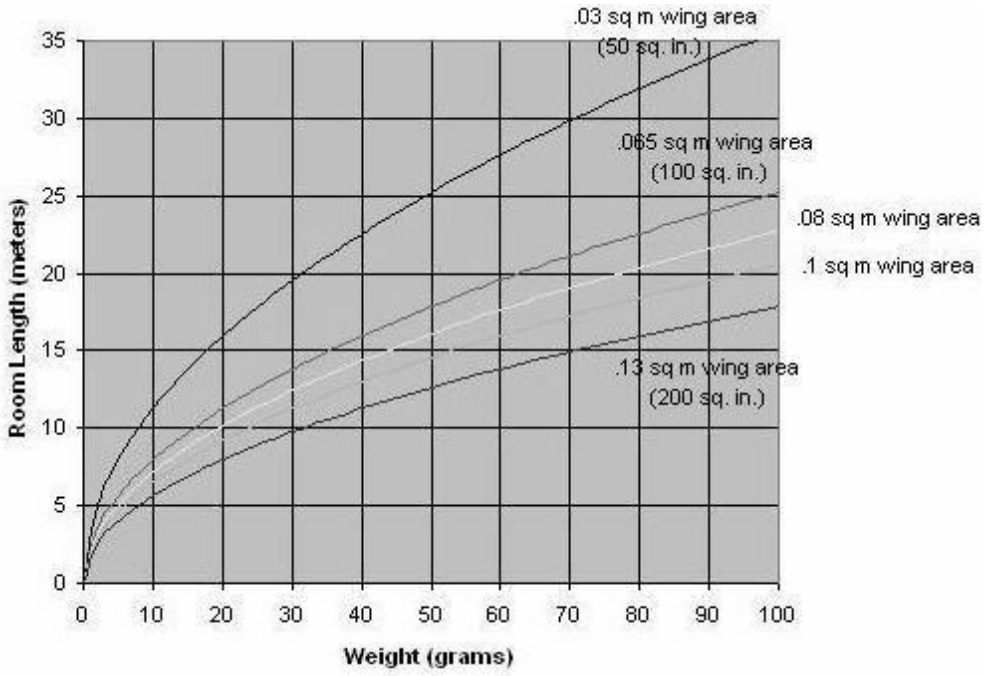

Fig. 8. Room size versus weight graph for different fixed-wing areas

camera's poor performance. We are currently testing more robust light-weight wireless cameras.

V. Sensor Suites for Flying Autonomously

Collision avoidance and the ability to takeoff and land are crucial in maneuvering through closed quarters. Infrared proximity sensors and ultrasonic sensors are often used by ground-based mobile robots to steer around obstacles [7]. The CQAR prototype has a minimum flying speed of 2 m/s and a turning radius of about 2.5 meters. To avoid large obstacles, it is preferable to detect them and initiate a turn at least two turning radii away (5 meters). This distance is generally out of range or accuracy of small, lightweight ultrasonic or infrared sensors. Processing of images captured by an aerial robot's on-board camera has been performed on outdoor aerial robots. Common methods exploit image features provided by the horizon [16] or flying field [20] which are both absent in closed quarters. The net effect is that conventional sensors and methods, although successful outdoors, have limitations indoors and thus demand alternative approaches.

Insect biologists confirm that flying insects like honeybees invoke optic flow for navigation. Optic flow is essentially the apparent visual motion experienced by an insect as it travels through the environment. Objects that are close will tend to appear to move faster than objects that are far away, and objects with which the insect are on a collision course will tend to appear as if they are rapidly increasing in size. Srinivasan observed that honeybees land by keeping the optic flow on the landing surface constant. Their group in Australia has successfully simulated optic flow based terrain-following and altitude control [18].

Figure 10 (top) depicts optic flow as it might be seen by an aerial robot traveling a straight line above the ground. The robot can estimate its height from the optic flow in the downward direction. The robot is able to detect the presence of obstacles by expansion in the forward direction. Through the use of multiple optic flow sensors, it is possible to estimate the aircraft's self-motion with respect to the Earth, including rotation information and sideslip.

Optic flow sensors, like those found in a PC mouse, are readily available. Centeye is one company that has been designing such sensors for autonomous collision avoidance on unmanned aerial vehicles [2]. Called the *Ladybug* and shown in Figure 10, the resulting sensor is composed of two parts: a mixed-mode "vision chip" images the environment and performs low-level processing using analog VLSI circuitry. Then an off-the-shelf microcontroller performs mid- and high-level processing using standard digital techniques. The resulting sensor, including optics, imaging, processing, and I/O weighs 4.8 grams. This sensor grabs frames up to 1.4 kHz, measures optic flow up to 20 rad/s, and functions even when texture contrast is just several percent. Such Ladybug sensors have been used to provide 1-meter outdoor RC aircraft with reliable autonomous altitude hold, terrain following, and obstacle detection.

A. Autonomous Takeoff and Landing

Optic flow can be used to autonomously land an aerial robot in closed quarters. This behavior demands the fixed-wing aircraft decrease forward speed V in proportion to altitude D.

$$OF = \frac{V}{D} \tag{2}$$

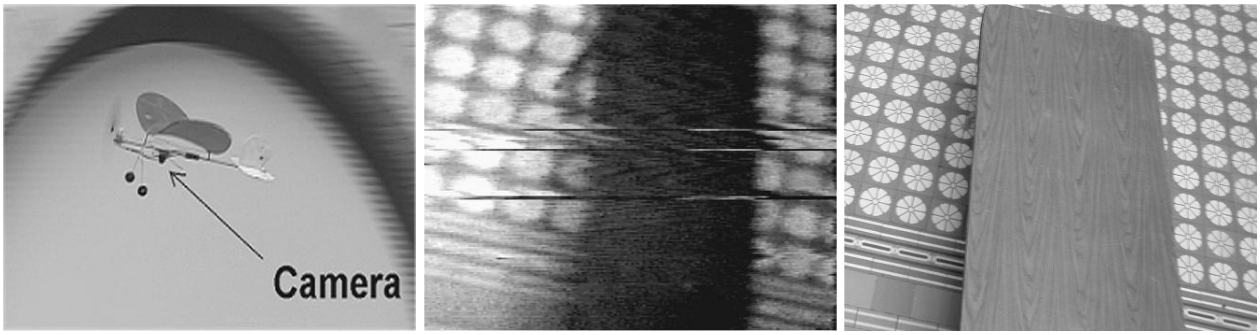

Fig. 9. An on-board wireless camera mounted on the flying prototype (left) can acquire video and transmit images (middle). Such images, although noisy, compare well with regular cameras (right).

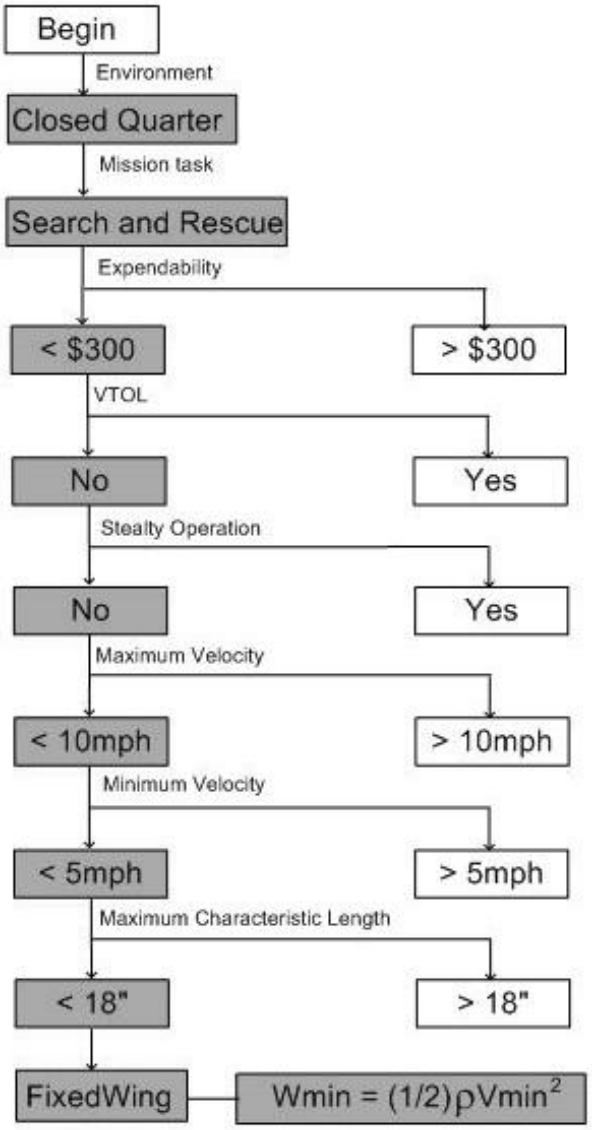

Fig. 7. Flow chart detailing execution of commands

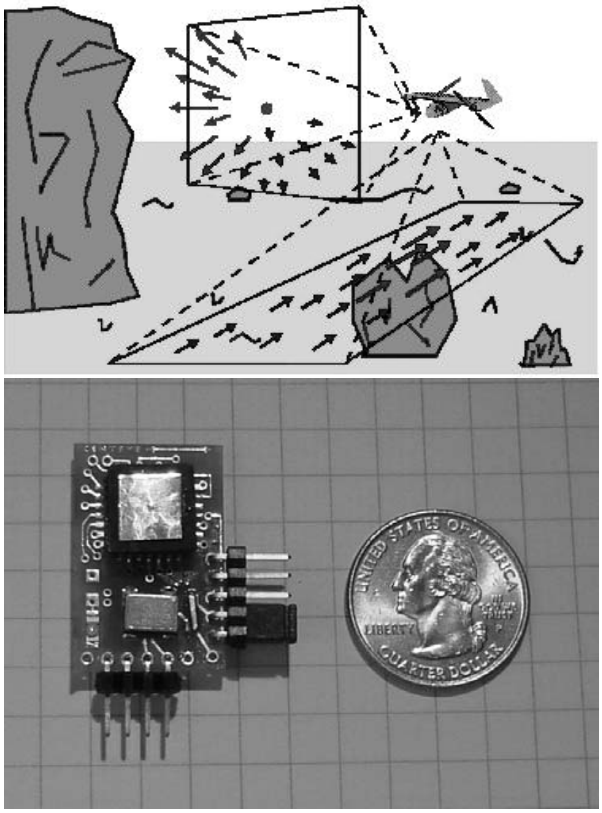

Fig. 10. Top: Optic flow as seen by an aerial robot flying above ground. Bottom: the mixed-mode VLSI optic flow microsensor is slightly bigger than a US quarter.

Keeping the optic flow OF in equation (2) constant, demands the aircraft's control system decrease forward speed in proportion to altitude and results in landing.

The optic flow control system block diagram and flow chart are shown in Figure 11. When approaching a landing, a microprocessor, or controller, will take an initial optic flow reading and set that as the desired value, $o_i(t)$. The controller will continue to take readings throughout the landing process and compute the error, $e(t)$, between the desired and actual values, $o_i(t)$ - $o_f(t)$. When the optic flow on the landing surface becomes larger than the desired optic flow, the error

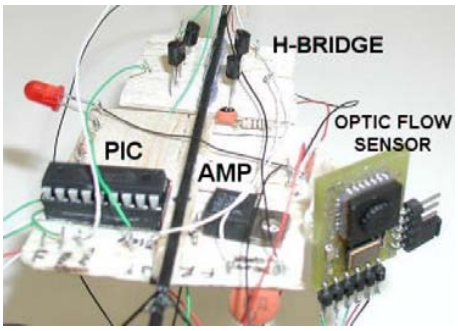

Fig. 12. A microcontroller is used to read the digital output of the optic flow sensor and implement the control algorithms. The control signal is then sent through an H-bridge to deflect the aircraft's control surfaces.

is negative and two conditions are possible. One, the forward velocity, v, could be significantly increasing. However, this is not likely during a landing sequence and can be ruled out. Two, the altitude, d, can be decreasing at a faster rate than v. Here, the controller will send a signal to the elevator, K_a, to slightly deflect it upwards to give a small increase in altitude. The other possibility is that the optic flow could start to dip below the desired level causing the error to be positive. The two possible cases that arise here are one, d is increasing but again this is not practical while in landing mode and two, v is decreasing faster than d. In this case, the controller will need to increase the propeller speed slightly by giving an output, K_m to the motor. After either control sequence has been implemented to force the optic flow back to the desired value, the throttle and elevator should be reset to its initial settings (i.e. K_a = K_m = 1).

An 8-bit PIC16F84 embedded microcontroller (see Figure 12), was used to implement the controller given in Figure 11 to gradually throttle down the motor while continuing to take readings throughout the landing process. The microcontroller issue pulse-width-modulated signals to adjust the thrust based on optic flow readings. This implementation yielded successful demonstrations of an autonomous landing (see Figure 13).

VI. Conclusions and Future Work

Closed quarters which are enclosed but spacious areas like warehouses, stadiums, underground parking lots and tunnels, are time consuming and labor intensive to patrol and safe keep. A robot designed to fly in closed quarters and deliver situational awareness would benefit homeland security, disaster mitigation and military operations. Applications could include biochemical detection, search-and-rescue and reconnaissance. This paper presented a working prototype based on output from a optimization matrix that parameterized design variables and introduced an optic flow based sensor for autonomous flight behaviors. Parameterization considered the pros and cons of different flight modes, namely lighter-than-air and both rotary and fixed wing aircraft. The resulting closed quarter aerial robot (CQAR) can fly safely and slowly in an area as small as 10×10 square meters and deliver wireless video with its on-board camera. A sensor suite that can achieve autonomous landing was demonstrated. Preliminary demos of autonomous collision avoidance flying indoors are promising. [9] [14].

References

[1] Anderson, J.D. (1999), *Aircraft Performance and Design*, McGraw-Hill.
[2] Barrows, G., Neely, C. (2000). "Mixed-mode VLSI Optic Flow Sensors for In-flight Control of a Micro Air Vehicle", *Proc. SPIE*, 4109 pp. 52-63.
[3] Blitch, J. (2002). "World Trade Center Search-and-Rescue Robots", Plenary Session *IEEE Int Conf Robotics and Automation*, Washington D.C.
[4] Choi, H., Sturdza, P., Murray, R.M. (1994). "Design and Construction of a Small Ducted Fan Engine for Nonlinear Control Experiments", *Proc. American Control Conf.*, Baltimore MD, pp. 2618-2622.
[5] Ettinger, S.M., Nechyba, M.C., Ifju, P.G., Waszak, M. (2002). "Vision-Guided Flight Stability and Control for Micro Air Vehicles", *IEEE/RSJ Int Conf on Robots and Systems*, Lausanne, Switzerland, pp. 2134-2140.
[6] Fearing, R., et al (2000). "Wing Transmission for a Micromechanical Flying Insect", *IEEE Int Conf Robotics and Automation*, San Francisco pp. 1509-1516.
[7] Flynn, A.M. (1988). "Combining Sonar and Infrared Sensors For Mobile Robot Navigation", *Int. Journal of Robotics Research*, pp. 5-14.
[8] Grasmeyer, J.M., Keennon, M.T. (2001). "Development of the Black Widow Micro Air Vehicle", *39th AIAA Aerospace Sciences Meeting and Exhibit*, Reno, NV.
[9] Green, W.E., Oh, P.Y., Barrows, G. (2004). "Flying Insect Inspired Vision for Autonomous Aerial Robot Maneuvers in Near-Earth Environments," *IEEE Int Conf on Robotics and Automation* (ICRA), New Orleans, V1, pp. 2347-2352.
[10] Kellog, J., et al (2001). "The NRL MITE Air Vehicle", *16th Bristol International Conference on Unmanned Air Vehicle Systems*, Bristol, UK.
[11] Kodiyalam, S., Sobieszczanski-Sobieski, J., "Multidisciplinary Design Optimization - Some Formal Methods, Framework Requirements, and Application to Vehicle Design", *Int. Journal of Vehicle Design (Special Issue)*, pp. 3-22.
[12] Hamel, T.; Mahony, R., Chriette, A. (2002). "Visual Servo Trajectory Tracking for a Four Rotor VTOL Aerial Vehicle", *IEEE International Conference on Robotics and Automation (ICRA)*, Washington, D.C., pp. 2781-2786.
[13] Nicoud, J.D., Zufferey, J.C. (2002). "Toward Indoor Flying Robots", *IEEE/RSJ Int Conf on Robots and Systems*, Lausanne, pp. 787-792.
[14] Oh, P.Y., Green, W.E. (2003). "Closed Quarter Aerial Robot Prototype to Fly In and Around Buildings", *Int. Conference on Computer, Communication and Control Technologies*, Vol. 5, pp. 302-307, Orlando, FL.
[15] Oh, P.Y., Green, W.E. (2003) "A Kite and Teleoperated Vision System for Acquiring Aerial Images", *IEEE International Conference on Robotics and Automation (ICRA)*, Taipei, Taiwan, pp. 1404-1409.
[16] Pipitone, F., Kamgar-Parsi, B., Hartley, R. (2001). "Three Dimensional Computer Vision for Micro Air Vehicles", *Proc. SPIE 15th Aerosense Symposium*, Conf. 4363, Enhanced and Synthetic Vision 2001, Orlando Florida.
[17] Sharp, C.S., Shakernia, O., Sastry, S.S. (2001). "A Vision System For Landing an Unmanned Aerial Vehicle *IEEE International Conference on Robotics and Automation (ICRA)*, Seoul, Korea, pp. 1720-1727.
[18] Srinivasan, M.V., Chahl, J.S., Weber, K., Venkatesh, S., Nagle, M.G., Zhang, S.W. (1998). *Robot Navigation Inspired By Principles of Insect Vision* in Field and Service Robotics, A. Zelinsky (ed), Springer Verlag Berlin, NY 12-16.
[19] Stone, H., Wong, K.C. (1997). "Preliminary Design of a Tandem-Wing Tail-Sitter UAV Using Multi-Disciplinary Design Optimization", *Int. Aerospace Congress*, Sydney, Australia pp. 707-720.
[20] Saripalli, S., Montgomery, J.F., Sukhatme, G.S. (2002). "Vision-based Autonomous Landing of an Unmanned Aerial Vehicle", *IEEE International Conference on Robotics and Automation (ICRA)*, Washington, D.C., pp. 2799-2804.
[21] Zhang, H., Ostrowski, J.P. (1999). "Visual Servoing With Dynamics: Control of an Unmanned Blimp", *IEEE International Conference on Robotics and Automation (ICRA)*, Detroit, pp. 618-623.

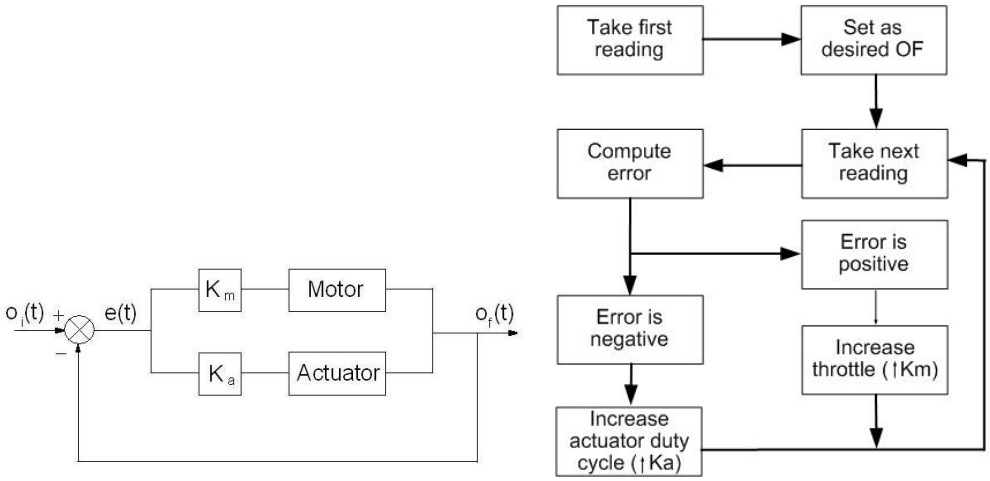

Fig. 11. Left: Optic flow control system block diagram. Right: Flow chart of how control system operates.

Fig. 13. The optic flow on the basketball gym floor is kept constant by the control system. That is, the aircraft (encircled) forward velocity is decreased in proportion with its altitude to land smoothly. Left: Aircraft just after hand launch. Middle: Aircraft midway through landing sequence at proportionally lower altitude and velocity. Right: Aircraft comes to a smooth landing within 25 $meters$ from starting point.

Paul Y. Oh received B.Eng. (Honors), M.Sc., and Ph.D degrees in mechanical engineering from McGill University (1989), Seoul National University (1992) and Columbia University (1999). His research interests include visual-servoing, mechatronics and aerial robotics. He was a Summer Faculty Fellow at the NASA Jet Propulsion Lab (2002) and the Naval Research Lab (2003). He is currently an assistant professor at Drexel University's Mechanical Engineering and Mechanics department. In 2004, he received a National Science Foundation CAREER Award. This Presidential Young Investigator award is for controlling micro air vehicles in near-Earth environments. He chairs the IEEE Technical Committee on Aerial Robotics for the Robotics and Automation Society.

William E. Green received a B.Sc. in Mechanical Engineering from Drexel University in 2002. He is a Dean's Fellow and currently pursuing a Ph.D in the Mechanical Engineering and Mechanics Program at Drexel University. His research interests include aerial robotics, mechatronics, and computer vision.